

## Effect of Sigma Phase Precipitation on the Pitting Corrosion Mechanism of Duplex Stainless Steels

Wang Yongqiang<sup>1</sup>, Sun Hao<sup>1</sup>, Li Na<sup>2\*</sup>, Xiong Yanhao<sup>1</sup>, Jing Hemin<sup>1</sup>

<sup>1</sup> School of Materials Science and Engineering, Anhui University of Technology, Maanshan, Anhui, 243002, China

<sup>2</sup> School of Metallurgical Engineering, Anhui University of Technology, Maanshan, Anhui, 243002, China

\* Corresponding author, E-mail: [linaustb@163.com](mailto:linaustb@163.com)

Received: 29 May 2018/ Accepted: 27 July 2018 / Published: 1 September 2018

---

A new phenomenon of the pitting corrosion of three duplex stainless steels (DSSs), SAF2205, SAF2507 and Z3CN20.09M, induced by sigma phases is found and discussed. The pitting potential ( $E_p$ ) of all three DSS specimens with smaller variations in the level of Cr content is remarkably higher than that of specimens with larger variations in Cr content, although they contain almost the same sigma precipitates. Even if there is much sigma phase in specimens with smaller variations in Cr content, they still present more resistance to pitting corrosion by high  $E_p$  values. The EIS results and microstructures of the DSS specimens after polarisation tests are in accordance with the potentiodynamic anodic polarisation results. The pitting of DSS induced by sigma precipitation is mainly ascribed to the level of difference in Cr content between the sigma phase and Cr-depleted zone and not only to the Cr-depleted zone itself.

---

**Keywords:** duplex stainless steel; sigma phase; Cr content difference; potentiodynamic polarisation; pitting corrosion

### 1. INTRODUCTION

Although stainless steels have extremely good general corrosion resistance that accounts for their countless diverse applications, they are nevertheless susceptible to localized corrosion, such as stress cracking corrosion, pitting corrosion and intergranular corrosion. Pitting corrosion, the localized dissolution of a passivated metal in the presence of a solution of certain anionic species, is a major cause of failure of metallic structures (stainless steels) due to pits that perforate or act as initiation sites for cracking[1]. Pitting corrosion has been described as random, covert, sporadic and abrupt, and the accurate prediction of the time and location of events remains extremely difficult. The evolution of corrosion pits on stainless steel has been known to occur in three distinct stages: nucleation, metastable

propagation and stable growth[2]. Any of these stages may be considered to be critical; nevertheless, the initiation step, which is essential to pitting, is most important. This stage is mainly a local breakdown of the passive film and is associated with the subsequent metastable pitting and stable growth. Once the passive film breaks down and a pit initiates, there is a possibility that a stable pit will grow[1].

Many contested models of pitting corrosion exist, but one undisputed aspect is that manganese sulphide inclusions play a critical role[3-7]. It is well-known that pitting on stainless steels starts preferentially at sulphide inclusions, notably at MnS particles physically associated with oxides due to their dissolution or chemical changes in and around sulphide inclusions, which induce the passive film breakdown[6, 8, 9]. However, the MnS theory may be invalid for some super clean steels containing very low sulphur impurity. In these steels, there is not sufficient MnS inclusion for sustaining the mass exchange inside and outside the pits during anodic reaction. Therefore, pit initiation induced by MnS is not ensured in these steels. Pitting corrosion is attributed to other factors. It should be noted that, whereas localized dissolution following breakdown of an otherwise protective passive film is the most common and technologically important type of pitting corrosion, pits can form under other conditions as well. For instance, pitting can occur during active dissolution if certain regions of the sample are more susceptible and dissolve faster than the rest of the surface[1, 10]. In fact, any factor that causes defects in passive film or chemical or physical heterogeneity at the surface, such as inclusions, second phase particles, solute-segregated grain boundaries, flaws, mechanical damage, or dislocations, is considered a possible reason for pitting corrosion. These factors can lead to a difference in property between different areas of the passive film and damage the protection of the passive film. Our previous work has shown that the micro-segregation of both chemical and secondary precipitated particles can degrade the pitting corrosion resistance of DSS[11-13]. In other studies, coincident conclusions have also been made[14-17]. Thus, another undisputed aspect is that secondary precipitates play an important role in the initiation of pitting corrosion of stainless steel.

Sigma, a hard and brittle Cr-rich phase, is one of the most common precipitates in duplex stainless steels (DSS) when exposed to temperatures ranging from 600-1000°C[18, 19]. It not only severely decreases the toughness of stainless steels but also negatively impacts localized corrosion resistance. Much work on the effect of sigma phase on the pitting corrosion of stainless steels has been done in the past decades[14, 16, 20, 21]. The occurrence of Cr-depleted zones around sigma phases has been undoubtedly considered as the mechanism for pit initiation known as “Cr-depleted theory”; however, some questions remain unclear. On the one hand, previous studies have indicated that the pitting corrosion resistance of DSS decreases with ageing time due to the increase of the sigma phase[22, 23]. However, with the increase of sigma phases, the difference in Cr concentration between Cr-depleted zones and sigma phases also enlarges owing to the strong dependence of the nucleation and growth of sigma on the uphill diffusion of Cr element, as the eutectoid decomposition of ferrite  $\alpha \rightarrow \sigma + \gamma_2$ . Therefore, the more important factor for pit initiation should be clarified. On the other hand, when the Cr content is above a certain threshold, the clusters of iron are finite, and dissolution proceeds for a while and then stops[2]. Thus, the critical level of Cr element that clearly induces pitting corrosion in a Cr-depleted zone should also be determined. This is a crucial step for understanding the

mechanism of the sigma effect on pitting corrosion to clarify these above problems. However, few attempts have been taken to focus on this in previous works.

In the present paper, three different DSS, SAF2205, SAF2507 and Z3CN20.09M, are adopted to elucidate the pitting mechanism induced by sigma precipitation. SAF2205 and SAF2507 are typical austenite( $\gamma$ )-ferrite( $\alpha$ ) duplex stainless steels widely used for energy, chemical petrochemical, and marine industries. The ratio of  $\alpha$  and  $\gamma$  is approximately 1:1. Meanwhile, Z3CN20.09M stainless steel is different from SAF2205 and SAF2507 and is characterized by a dual-phase microstructure in which less  $\alpha$ -ferrite phase is distributed in the  $\gamma$ -austenite matrix. There are also differences in chemical composition and microstructure among SAF2205, SAF2507 and Z3CN20.09M DSS. The investigation results of different DSS can be more convincing.

## 2. MATERIALS AND EXPERIMENTAL

### 2.1 Materials

Three types of duplex stainless steels, SAF2205, SAF2507 and Z3CN20.09M, were adopted, and their chemical compositions are listed in Table 1.

**Table 1.** Chemical compositions of three duplex stainless steels (wt.%).

Type	Elements(wt%)									
	C	Si	Mn	P	S	Cr	Ni	Mo	N	Fe
SAF2205	0.023	0.38	1.35	0.026	0.001	22.07	4.83	2.37	0.19	balance
SAF2507	0.023	0.497	1.55	0.020	0.001	25.15	7.37	4.35	0.25	balance
Z3CN20.09M	0.027	1.27	1.13	0.023	0.0009	20.19	8.92	0.21	0.031	balance

**Table 2.** Heat treatment technique of three duplex stainless steels.

Samples	Heat treatment technique	Heat treatment temperature	Heat treatment time/h	Cooling method
	solid solution	1050°C	0.5	
SAF2205	aging	850°C	3.5, 4, 6, 9, 10, 14, 20, 24, 30	quenching
	aging + annealing	850°C for 30 h + 950°C	0.08, 0.33	
	solid solution	1100°C	0.5	
SAF2507	aging	800°C	0.25, 0.33, 0.42, 0.5, 0.75, 1, 1.5, 2	quenching
	aging + annealing	800°C for 1 h + 1000°C	0.08, 1.08	

Z3CN20.09M	solid solution aging	1180°C 750°C	0.5 4, 10, 12, 22, 24, 50, 100	quenching
	aging + annealing	750°C for 50 h + 860°C 750°C for 100 h + 860°C	0.5 0.25, 0.5, 1	

SAF2205, SAF2507 and Z3CN20.09M DSS were respectively annealed at 1050°C, 1100°C, 1180°C for 0.5 h for the solid solution first. Then, the three different DSS were aged at different temperatures for different times to obtain different amounts of sigma phase. Furthermore, some of the aged DSS samples were annealed at high temperature for a certain time for acquiring different Cr concentrations in the Cr-depleted zone. The detailed heat treatment parameters are shown in Table 2.

## 2.2 Microstructure examination

The three annealed and aged DSS were cut into small specimens with a size of 10 × 10 × 10 mm for revealing the microstructure and examining the pitting corrosion resistance. The specimens were abraded using silicon carbide abrasive paper to 2000# and then polished by diamond paste with a size of 1.5 μm. Finally, the specimens were electrochemically etched for 10-20 s in a 20 wt% NaOH solution in distilled water with a direct voltage of 3 V in order to differentiate the ferrite, austenite and sigma phases. The microstructures of the specimens were observed by optical microscopy (OM) and scanning electron microscopy (SEM). The ferrite content and volume fraction of the sigma phases of the specimens were calculated on 20 optical measurements for each specimen by using a quantitative metallography analysis software (Image-Pro Plus 6.0).

## 2.3 Micro-composition examination

Aged and annealed specimens were abraded using silicon carbide abrasive paper to 2000# and then polished by diamond paste with a size of 1.5 μm; finally, they were rinsed in distilled water, ultrasonically cleaned in anhydrous alcohol and dried in air for examination of the composition of sigma phases and Cr-depleted zones. The quantitative compositions of the sigma phases and Cr-depleted zones in the specimens were measured by the energy dispersive spectrometer (EDS) in the SEM using the backscattered electron (BSE) technique.

## 2.4 Electrochemical measurements

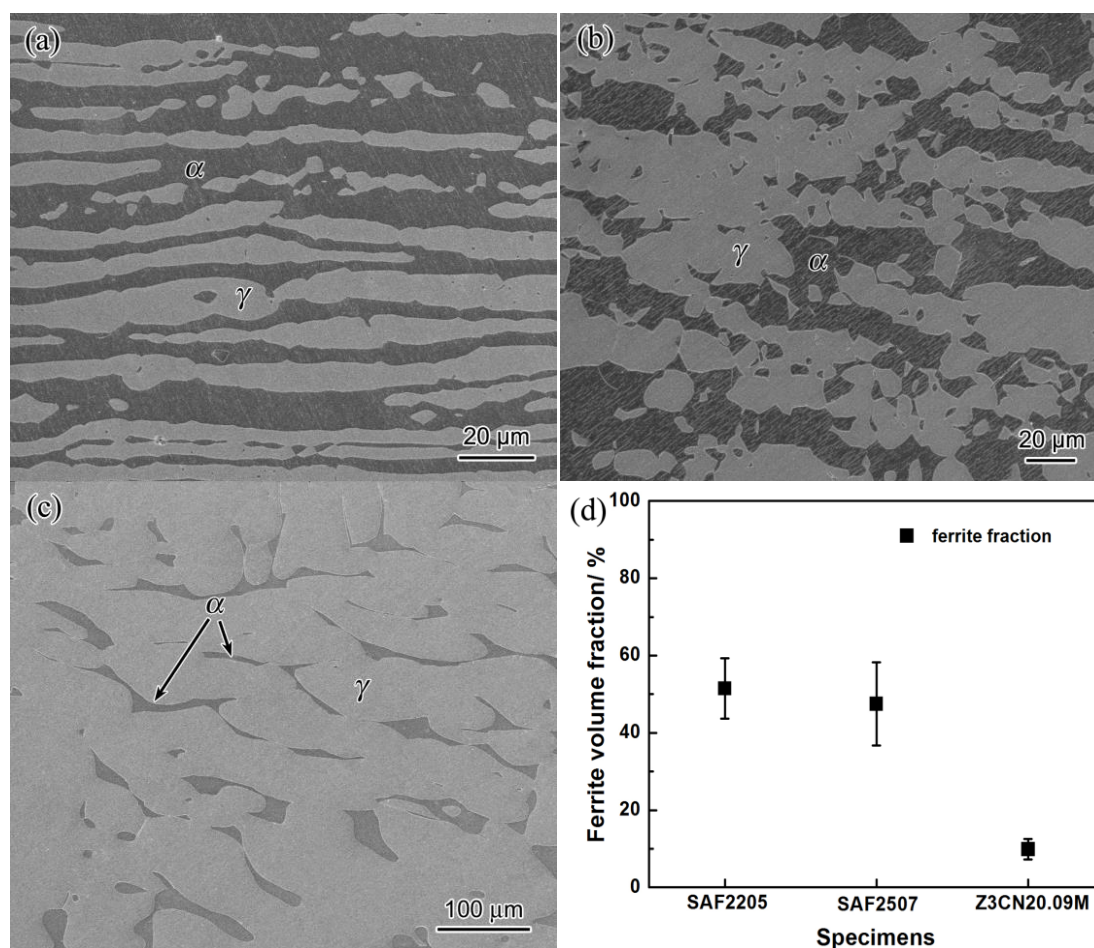
DC electrochemical measurements were performed with an electrochemical workstation. Three DSS specimens with a size of 10 × 10 × 3 mm were used as working electrodes and were prepared by spot welding a copper wire onto one side of each specimen and then embedding the specimen in epoxy resin with an exposure area of 1 cm<sup>2</sup>. The reference electrode was a saturated calomel electrode (SCE), and a Pt foil was used as the auxiliary electrode.

Pitting corrosion studies were carried out in a  $0.5 \text{ mol}\cdot\text{L}^{-1}$  NaCl solution at constant temperature ( $30\pm 1^\circ\text{C}$ ) by potentiodynamic anodic polarisation and electrochemical impedance spectroscopy (EIS) techniques to evaluate the pitting potential ( $E_p$ ) and the passive layer breakdown of the specimens, respectively.  $E_p$  is defined as the potential at which the current increases sharply from the passive current level[1].

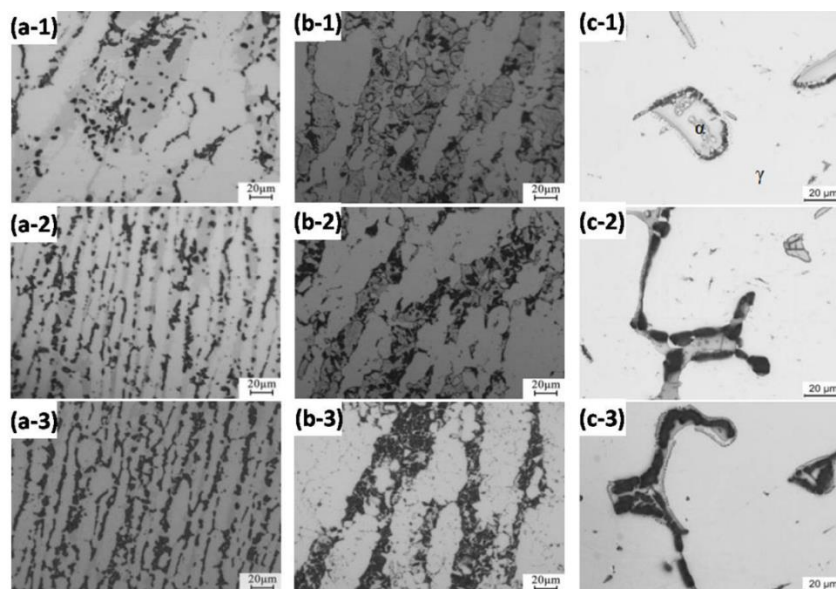
Before testing, the working electrodes were immersed in the test solution for 15 min until steady-state open circuit potential (OCP) was reached. In addition, a potential sweep was applied in the anodic direction at a scan rate of  $20 \text{ mV}\cdot\text{min}^{-1}$  from  $-400 \text{ mV}$  (SCE) to an appropriate value. EIS measurements were carried out using the frequency range of 100 kHz to 0.01 Hz at the OCP. Amplitudes of all sinusoids were equal to 10 mV. The EIS results were interpreted by using an equivalent circuit. The characteristic parameter values of these elements in an equivalent circuit were then obtained directly by fitting the experimental curves using Zview Version 3.1<sup>®</sup> software.

### 3. RESULTS AND DISCUSSION

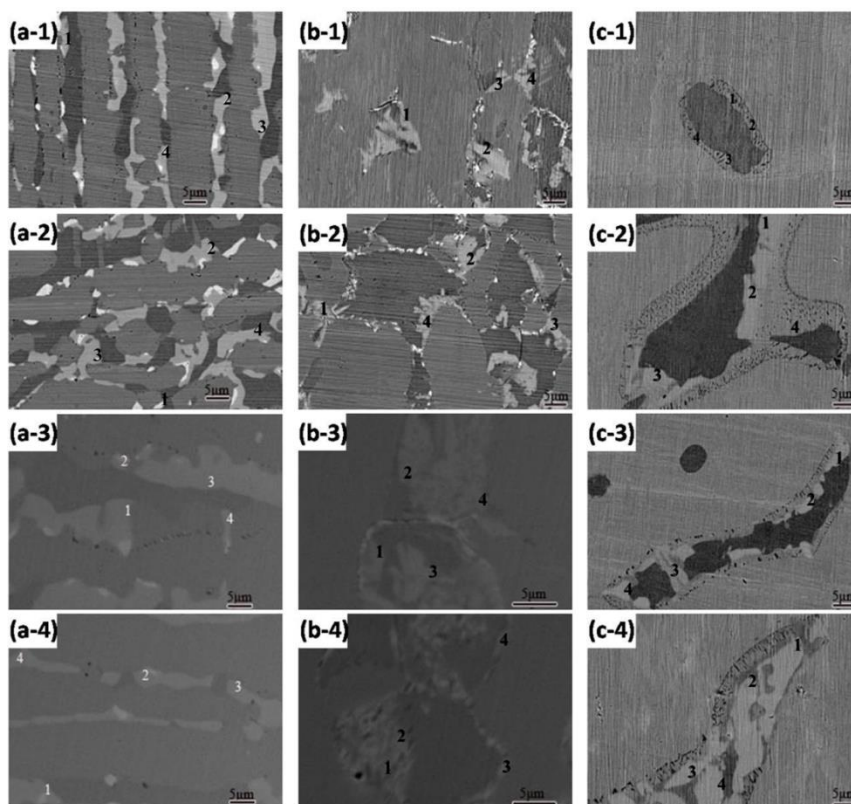
#### 3.1 Microstructures and micro-composition of the three DSS specimens



**Figure 1.** Microstructures of different specimens: (a) SAF2205, (b) SAF2507, and (c) Z3CN20.09M; (d) the statistics of ferrite content.

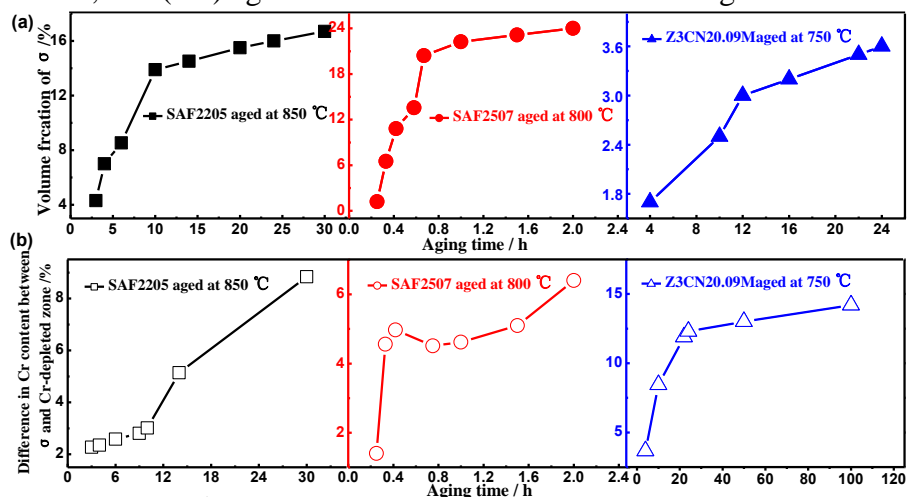


**Figure 2.** Microstructures of different specimens: (a) SAF2205 aged at 850°C for (a-1) 3.5 h, (a-2) 9 h, and (a-3) 30 h; (b) SAF2507 aged at 800°C for (b-1) 0.33 h, (b-2) 0.42 h, and (b-3) 1 h; and (c) Z3CN20.09 M aged at 750°C for (c-1) 4 h, (c-2) 24 h, and (c-3) 100 h.

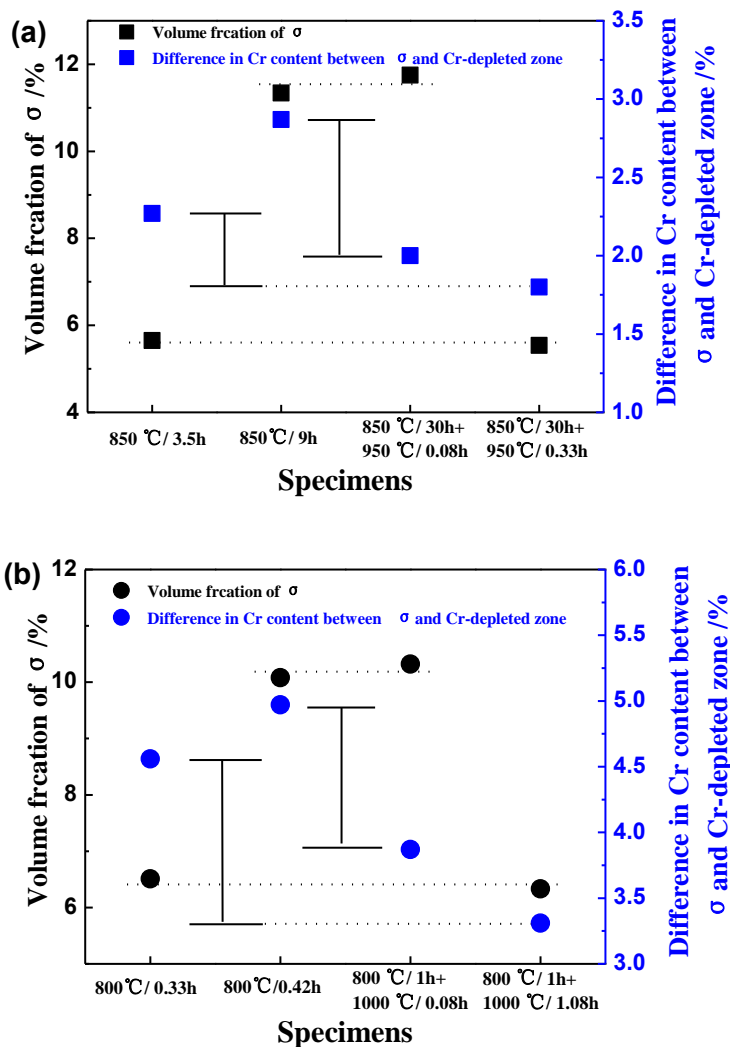


**Figure 3.** SEM micrographs of different DSS specimens: (a) SAF2205, (b) SAF2507 and (c) Z3CN20.09M examined by BSE model. (a-1) and (a-2) aged at 850°C for 3.5 h and 9 h, respectively; (a-3) and (a-4) aged at 850°C for 30 h after annealing at 950°C for 0.08 h and 0.33 h, respectively; (b-1) and (b-2) aged at 800°C for 0.33 h and 0.42 h, respectively; (b-3) and (b-4) aged at 800°C for 1 h after annealing at 1000°C for 0.08 h and 1.08 h, respectively; (c-1) and

(c-2) aged at 750 °C for 4 h and 10 h, respectively; (c-3) aged at 750 °C for 50 h after annealing at 860 °C for 0.5 h, and (c-4) aged at 750 °C for 100 h after annealing at 860 °C for 1 h.



**Figure 4.** Volume fraction of sigma phases (a) and difference in Cr content between the sigma phase and Cr-depleted zone (b) in three aged DSS specimens.



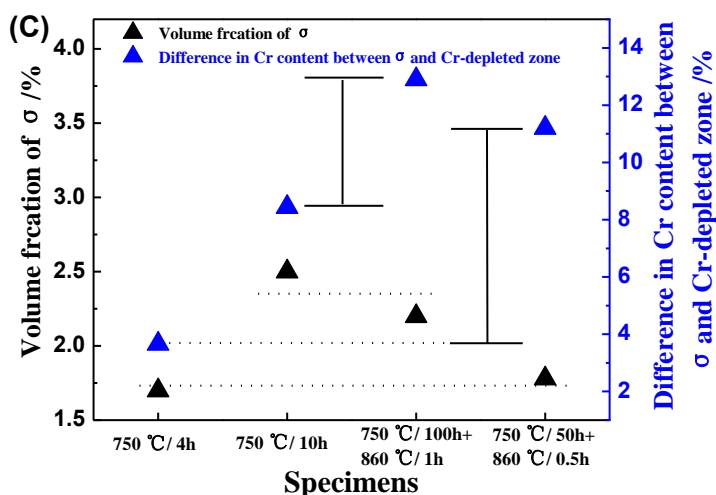


**Figure 5.** Different in Cr content between the sigma phase and Cr-depleted zone in three DSS specimens with nearly the same amount of sigma phase: (a) SAF2205, (b) SAF2507 and (c) Z3CN20.09M specimens.

Fig. 1 shows the microstructures of solid solution SAF2205, SAF2507 and Z3CN20.09M DSS specimens, which consist of both austenite (grey) and ferrite (dark) phases. No other phase is observed in these specimens.

Moreover, the volume fractions of ferrite phase in three DSS specimens are approximately 51.5%, 47.5% and 9.9%, respectively (Fig. 1d). The ratios of austenite and ferrite phases are determined by Cr and Ni equivalents of stainless steel[24]. The microstructures of the aged specimens are shown in Fig. 2. Fig. 3 shows the SEM micrographs of different aged and annealed DSS specimens examined using the BSE signal model, and the Arabic numbers in the figure are the examination positions of the elemental contents by EDS. The sigma phase formed in the ferrite of DSS following the decomposition:  $\alpha \rightarrow \sigma + \gamma_2$ ; the formation is mainly controlled by Cr diffusion and belongs to diffusion phase transformation[25, 26]. Therefore, the number of sigma phases in all three DSS aged at different temperatures increased with ageing time (Fig. 4a). Meanwhile, it can be concluded that Cr concentration in and around the sigma phase changes with the precipitation and growth of the sigma phase and that the difference in Cr content between the sigma phase and secondary austenite (Cr-depleted zone) increases with ageing time due to the continuous diffusion of Cr into the sigma phase (Fig. 4b).

It is well known that the precipitation of sigma phase in DSS occurs in a certain range of temperature; when temperature exceeds the highest value, the sigma phase dissolves gradually due to its thermodynamic instability. For example, the temperature range of sigma formation in SAF2205 DSS is generally between 700 and 900°C[25]. According to previous work, the solid solution temperatures of the sigma phase in Z3CN20.09M, SAF2205 and SAF2507 DSS are 850°C, 950°C, and 1000°C, respectively[18, 25, 26]. Thus, the sigma phase in the three DSS specimens annealed at 860°C, 950°C, 1000°C after ageing decreased with annealing time. As a result, nearly the same amount



of sigma phase was achieved in specimens with different variations in Cr content between the sigma phase and Cr-depleted zone using appropriate annealing and ageing techniques, as shown in Fig. 5.

3.2 Potentiodynamic anodic polarisation curves of aged DSS specimens

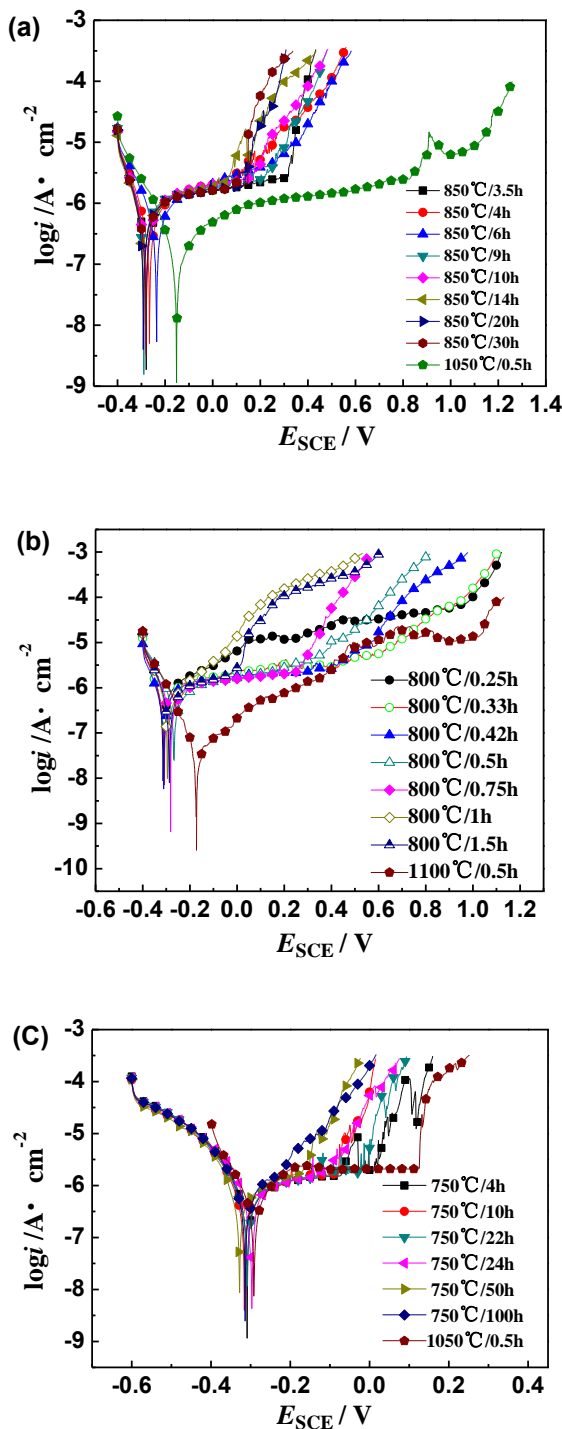


**Figure 6.** Potentiodynamic anodic polarisation curves of different aged DSS specimens tested in 0.5 mol L<sup>-1</sup> NaCl solution: (a) SAF2205, (b) SAF2507 and (c) Z3CN20.09M.

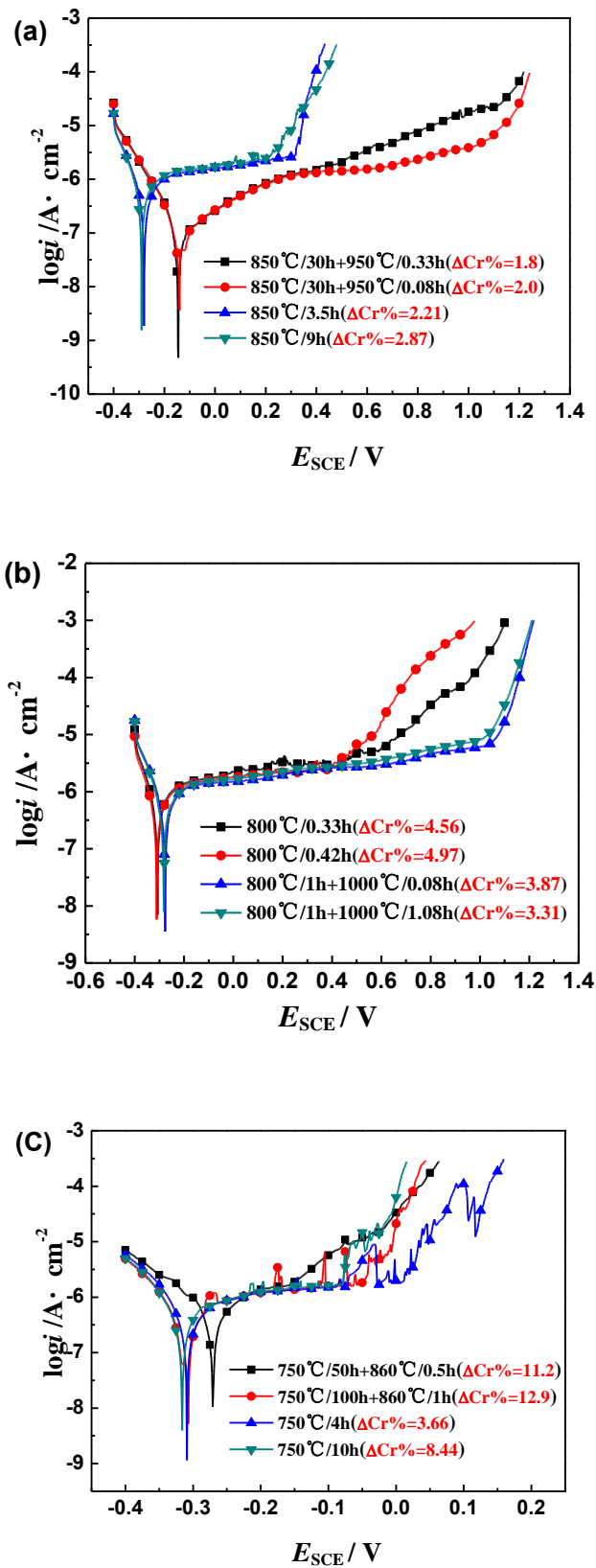
Fig. 6 shows the polarisation curves of three different DSS specimens immersed in 0.5 mol L<sup>-1</sup>NaCl solution. Based on the polarisation curves, the variation in pitting potential ( $E_p$ ), corrosion potential ( $E_{corr}$ ) and corrosion currents ( $I_{corr}$ ) of the specimens can be found, as shown in Table 3.

**Table 3.** Potentiodynamic polarisation parameters of three DSS specimens in 0.5 mol·L<sup>-1</sup>NaCl solution.

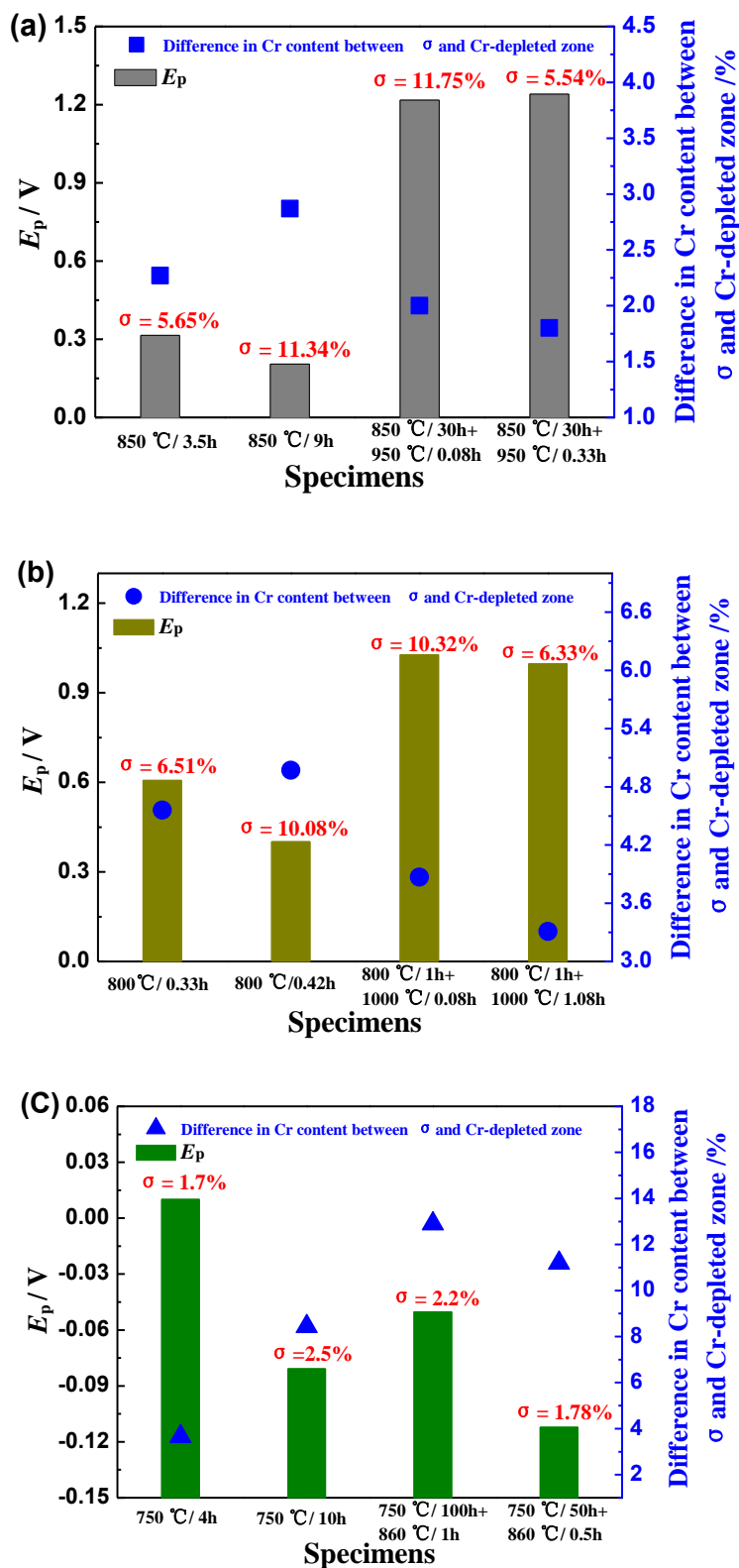
Specimens	Heat treatment (T/h)	$E_p/V$	$E_{corr}/V$	$\log(i_{corr}/A)$
SAF2205	1050°C/0.5	1.122	-0.1549	2.044e-007
	850°C/3.5	0.315	-0.2817	6.514e-007
	850°C/9	0.205	-0.2916	6.106e-007
	850°C/20	0.130	-0.2949	5.979e-007
	850°C/30	0.096	-0.2811	5.906e-007
SAF2507	1100°C/0.5	1.036	-0.1771	5.882e-008
	800°C/0.25	0.962	-0.3170	4.180e-007
	800°C/0.33	0.600	-0.3098	6.964e-007
	800°C/0.42	0.400	-0.3128	3.980e-007
	800°C/0.75	0.255	-0.2832	6.034e-007
Z3CN20.09M	1050°C/0.5	0.122	-0.2945	3.972e-007
	750°C/4	0.010	-0.3095	9.511e-007
	750°C/10	-0.081	-0.3165	9.181e-007
	750°C/24	-0.124	-0.2987	9.650e-007
	750°C/50	-0.152	-0.3285	1.153e-006

It can be seen that  $E_p$  decreased with ageing time, which is consistent with the increase of sigma in the specimens with ageing time. It suggests that the pitting resistance of the three aged DSS specimens becomes worse with the increase of ageing time. Clearly, the decrease in pitting corrosion resistance in the aged specimens is directly attributed to the formation of sigma phases. The pitting corrosion resistance of duplex stainless steel is significantly affected by metallurgical variables, such as microstructure, inclusions, precipitates, alloy composition and heat treatment[1, 11, 27] Certain precipitated phases can act as sites for the preferential initiation of pits, whereas others can cause micro-segregation, such as depletions, of chromium, nitrogen and molybdenum. Clearly, the depleted zones induce pits on the steel surface. As mentioned previously, the formation of sigma phase in the three DSS causes the Cr-depleted zone. The interface between the Cr-rich precipitates and secondary austenite becomes the preferential site for pit initiation; subsequently, pits grow in the secondary austenite (Cr-depleted zone)[20, 23]. Therefore, the pitting corrosion resistance of the three DSS specimens decreased with increasing sigma phase. However, with the increase of sigma phases, the difference in Cr concentration between Cr-depleted zones and sigma phases also enlarges owing to the nucleation and growth of sigma that is strongly dependent on the uphill diffusion of Cr element, as the eutectoid decomposition of ferrite is  $\alpha \rightarrow \sigma + \gamma_2$ . Therefore, more important factors for pit initiation should be discussed and clarified.

Fig. 7 displays the polarisation curves of the three DSS specimens with different variations in Cr content between the sigma phase and Cr-depleted zone but with nearly the same amount of sigma phase. Based on the polarisation curves, the variation in pitting potential ( $E_p$ ) for the different DSS specimens can be found, as shown in Fig. 8. The pitting potential of SAF2205 specimens aged at 850°C for 3.5 h is remarkably lower than that of specimens aged at 850°C for 30 h after annealing at 950°C for 0.33 h, although these two SAF2205 DSS specimens contain almost the same sigma precipitates.



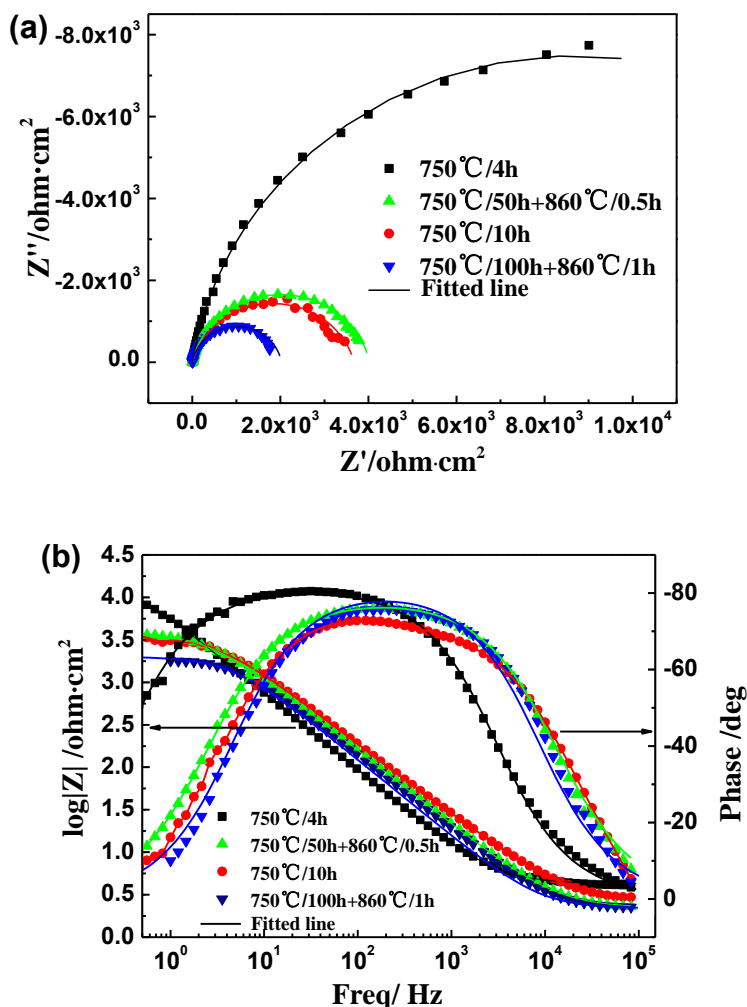
**Figure 7.** Potentiodynamic anodic polarisation curves of different aged and annealed DSS specimens tested in  $0.5 \text{ mol L}^{-1} \text{NaCl}$  solution: (a) SAF2205, (b) SAF2507 and (c) Z3CN20.09M.



**Figure 8.** Variation in pitting potential as the difference in Cr content between sigma and Cr-depleted zone and number of sigma phase in different DSS specimens: (a) SAF2205, (b) SAF2507 and (c) Z3CN20.09M.

This trend of  $E_p$  was also found in the SAF2507 and Z3CN20.09M specimens. During upward scanning in a polarisation experiment, a stable pit starts growing at  $E_p$ . It is generally considered that materials exhibiting higher values of  $E_p$  are more resistant to pitting corrosion[1]. Therefore, the pitting resistance of specimens with smaller variations in Cr content between the sigma phase and Cr-depleted zone is better than that of specimens with higher variations in Cr content, although the specimens contain more sigma phases; for example, the SAF2205 specimens were aged and annealed at 850 °C/30 h + 950°C/0.08 h, respectively, and the SAF2507 specimens were aged and annealed at 800°C/1 h + 1000°C/0.08 h, respectively. It indicates that the degree of Cr depletion is more sensitive to the pitting corrosion of DSS than the number of Cr-depleted zones. In other words, pitting induced by sigma precipitation is mainly ascribed to the level of difference in Cr content between the sigma phase and Cr-depleted zone and not only to the Cr-depleted zones. In addition, more sigma phases do not always lower the pitting resistance of DSS. Higher resistance to pitting corrosion can be obtained in DSS containing more sigma phases. Therefore, there is no certain relationship between resistance to pitting corrosion and number of sigma phases.

3.3 EIS results of aged DSS specimens



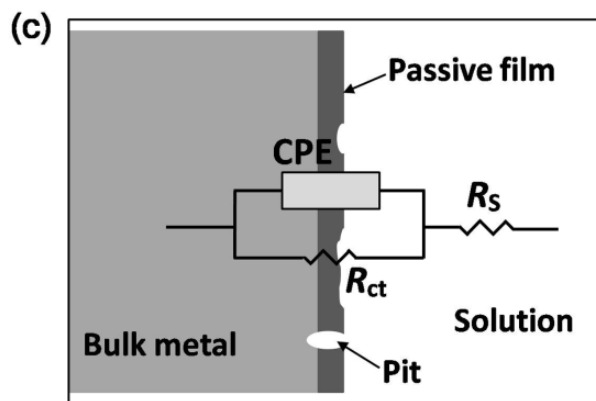


**Figure 9.** The effect of Cr content difference on the (a) Nyquist and (b) Bode plots of Z3CN20.09M specimens measured at open circuit potential with a sinusoidal potential amplitude of 10 mV, running from 100 kHz to 10 mHz in the 0.5 mol L<sup>-1</sup>NaCl solution at room temperature. (c) Equivalent circuit representative of the electrode interface for the Z3CN20.09M specimens in the 0.5 mol L<sup>-1</sup>NaCl solution.

Fig. 9 displays the EIS results of different aged and annealed Z3CN20.09M specimens, indicating the effect of Cr content difference on the Nyquist and Bode plots of Z3CN20.09M specimens in 0.5 mol L<sup>-1</sup>NaCl solution at OCP. One can see that the Nyquist plots are all semi-circular arcs with centres depressed below the x-axis. This type of diagram is usually interpreted as a mechanism of charge transfer on an inhomogeneous surface[28]. Distinct differences in the semicircle arcs for the different specimens in the Nyquist plots can be observed in the figure. With increasing Cr content difference, the diameter of the depressed semicircle decreases. In general, an increase in the semicircle arc radius indicates an increase in the charge-transfer resistance ( $R_{ct}$ ) value, which is inversely proportional to the corrosion rate of the system. The semicircle arc radius values of the specimens with smaller variations in Cr content, for example, those aged at 750°C for 4 h, are significantly larger than those of the specimens with larger variations in Cr content (those aged at 750°C for 100 h after annealing at 860°C for 1 h). It means that the charges in the specimens transfer with difficulty through the passive film of the specimens with smaller variations in Cr content.

An equivalent electrical circuit was designed as a best-fit to the experimental results and is displayed in Fig. 8(c). The circuit is composed of an arrangement of [ $R_s(\text{CPE}||R_{ct})$ ] elements, where  $R_s$  is the solution resistance and CPE is the constant phase element in parallel connection with  $R_{ct}$ , which is the charge-transfer resistance at the interface. The impedance expression of CPE[29],  $Z_{\text{CPE}}$ , is given by

$$Z_{\text{CPE}} = T^{-1}(j\omega)^{-n}(1)$$

where  $\omega$  is the angular frequency,  $j$  is the imaginary unit,  $T$  is the proportionality factor,  $n$  is the phase shift,  $j = (-1)^{1/2}$ , and  $\omega = 2\pi f$ , where  $f$  is the frequency (Hz). The CPE exponent,  $n$ , is a measure of capacitance dispersion with values between 1 (ideal capacitance) and 0.7 (highly dispersed capacitance, such as at porous electrodes). For  $n = 0$ ,  $Z_{\text{CPE}}$  represents resistance with  $R = T^{-1}$ ; for  $n = 1$ , it represents capacitance with  $C = T$ ; for  $n = 0.5$ , it represents the Warburg element; and for  $n = -1$ , it represents inductance with  $L = T^{-1}$  [30]. The theoretically simulated impedance parameters for the Z3CN20.09M specimens are computed and listed in Table 4.

From the table, higher  $R_{ct}$  values are observed in the specimens containing small variations in Cr content, followed by the specimens containing large variations in Cr content.  $R_{ct}$  decreased and reached the lowest value in the specimen aged at 750°C for 100 h after annealing at 860°C for 1 h, with a maximum of 12.9% in Cr content difference.

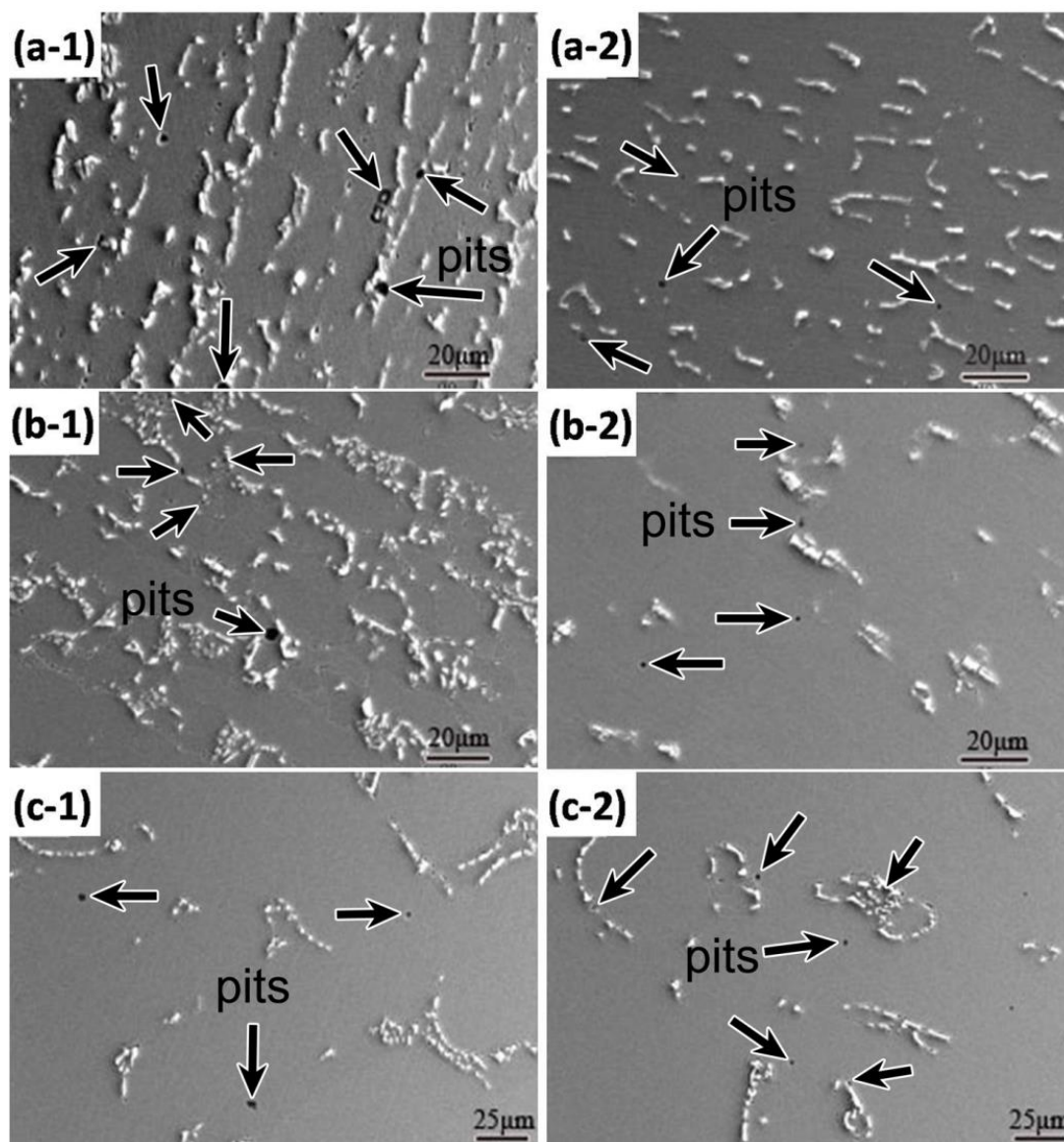
**Table 4.** Equivalent-circuit element values for EIS data corresponding to Z3CN20.09M specimens aged and annealed in the 0.5 mol L<sup>-1</sup>NaCl solution.

specimens	$R_s$ ( $\Omega$ cm <sup>2</sup> )	CPE-T/F cm <sup>2</sup>	CPE-n	$R_{ct}$ ( $\Omega$ cm <sup>2</sup> )
750°C/4 h	4.258	2.1062E-5	0.90605	17349
750°C/50 h+860°C/0.5 h	2.217	2.2236E-5	0.87582	4022
750°C/10 h	2.758	2.3181E-5	0.84339	3671
750°C/100 h+860°C/1 h	2.176	2.3726E-5	0.90553	2014

The lower  $R_{ct}$  value represents an increased transport of ions through the double-charge layer, which indicates relatively poor resistance to corrosion. Therefore, the specimens with a maximum Cr content difference of 12.9% had the worst resistance to corrosion. Moreover, the specimen also had the highest CPE-T value among all specimens, suggesting that its passive film presented the worst stability[31]. The same tendency of EIS results were also obtained for the SAF2205 and SAF2507 DSS specimens.

In general, the passive film on the surface of stainless steels is determined by the alloy composition, electrolyte media, and condition of the material[1,32]. Cr is considered the most important element in conferring passivity to stainless steels[33]. The pitting potential of stainless steels is correspondingly found to increase dramatically as the Cr concentration increases[34]. The precipitation of sigma phase enriched in Cr element in the ferrite of DSS brings the segregation of Cr concentration on the alloy surface. This results in two thermodynamic and kinetics problems of pitting corrosion. On the one hand, the electric potential of the sigma phase is higher than that of secondary austenite phase (Cr-depleted zone) due to the higher Cr content in sigma phase. Therefore, there is a difference in pitting thermodynamics between the sigma phases and Cr-depleted zones and in inducing the formation of micro-galvanic cells on the stainless steel surface. On the other hand, the heterogeneous passive film including thick and/or nonuniform composition generated on the stainless steel surface is caused by the segregation of Cr concentration. The drawback is that the passive film breaks easily and the transport of aggressive Cl<sup>-</sup> ions through the passive film to the metal/oxide interface becomes easy. In addition, the probability of chloride adsorption and film thinning is also much higher. The higher the difference in Cr content between the sigma phase and Cr-depleted zone is, the worse the heterogeneity of the passive film and the poorer the resistance to pitting corrosion. Thus, the Z3CN20.09M specimens aged at 750 °C for 50 h after annealing at 860 °C for 0.5 h with approximately 11.2% Cr content difference have poorer pitting corrosion resistance than that of specimens aged at 750 °C for 4 h with less than 3.66% Cr content difference, although they contain nearly the same sigma phases.

## 3.4 SEM micrographs of DSS specimens after polarisation tests.



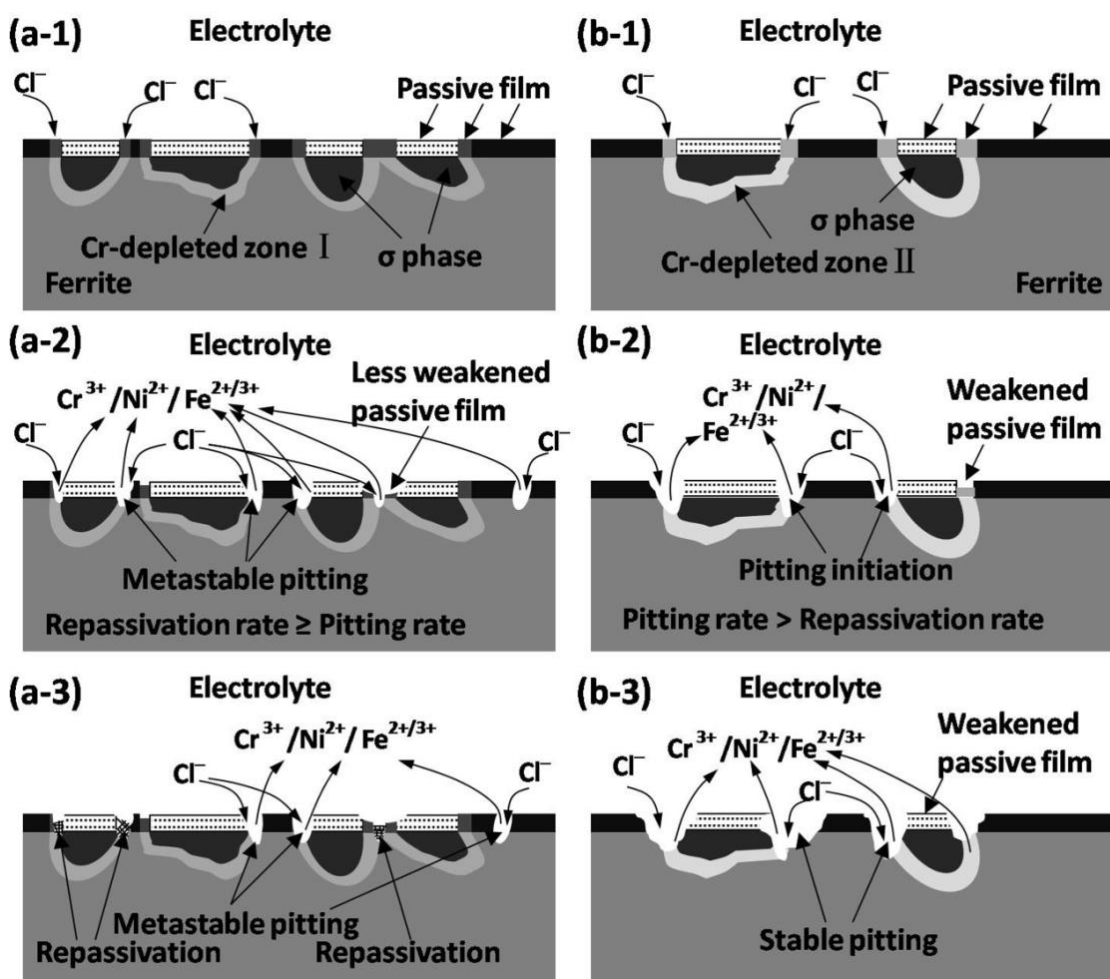
**Figure 10.** SEM microstructures of (a) SAF2205, (b) SAF2507 and (c) Z3CN20.09M DSS aged and annealed specimens after polarisation testing in the 0.5 mol L<sup>-1</sup>NaCl solution at room temperature. (a-1) aged at 850°C for 9 h, (a-2) aged at 850°C for 30 h after annealing at 950°C for 0.08 h; (b-1) aged at 800°C for 0.42 h, (b-2) aged at 800°C for 1 h after annealing at 1000°C for 1.08 h; (c-1) aged at 750°C for 4 h, (c-2) aged at 750°C for 50 h after annealing at 860°C for 0.5 h.

Fig. 10 shows the SEM microstructures of SAF2205, SAF2507 and Z3CN20.09M DSS specimens after polarisation tests. It can be seen that in specimens with larger variations in Cr content, for example, the SAF2205 specimens aged at 850°C for 9 h, more pits arose at and/or in the boundaries of austenite and ferrite in which the sigma phase precipitated (seen in Fig. 10(a-1)). However, in other specimens with smaller variations in Cr content, for example, the SAF2205 specimens aged at 850°C for 30 h after annealing at 950°C for 0.08 h, fewer pits appeared at and/or in the boundaries of



austenite and ferrite, although these specimens contained more sigma phases (seen in Fig. 10(a-2)). The same results as those for SAF2205 specimens were obtained for the SAF2507 and Z3CN20.09M specimens, as shown in Fig. 10(b) and (c). The high probability of pitting corrosion of specimens with larger variations in Cr content occurring at and/or in the boundaries of austenite and ferrite indicates that the difference in the level of Cr content is more important than the amount of sigma phases (or Cr-depleted zones). This accords with the electrochemical measurement results and supports the above tests.

### 3.5 Pitting corrosion mechanism of DSS induced by sigma precipitation.



**Figure 11.** Schematic illustration of comparing the pitting corrosion process of the DSS specimen between those with smaller variations in the level of Cr content (a) and those with larger variations in the level of Cr content (b) during potentiodynamic polarisation. (a-1) and (b-1) the  $\text{Cl}^-$  ions prefer to attack the defects of passive film; (a-2) and (b-2) the protectiveness of the passive film is weakened and then lost, pits initiate, and the dissolution within the pits draws  $\text{Fe}^{2+/3+}$ ,  $\text{Cr}^{3+}$ ,  $\text{Ni}^{2+}$ , and  $\text{Cl}^-$  ions by electro-migration, weakening the surrounding passive film; (a-3) re-passivation occurred in specimens with smaller variations in the level of Cr content due to lower composition micro-segregation of Cr element, which induces a certain degree of protection of the passive film; (b-3) a large variation in the level of Cr content weakened the passive film and resulted in the stabilization of pitting.

Fig. 11 shows the schematic illustration comparing the process of pitting corrosion induced by sigma precipitation in DSS specimens with larger and smaller variations in the level of Cr content. There are three stages of pitting: passive film breakdown, metastable pitting and pit growth. The passive state is required for pitting to occur. The passive film must be formed on the surface of the alloy before pitting occurs; meanwhile, re-passivation still exists during the process of pitting under a certain potential. When the rate of re-passivation is higher than that of passive film thinning or dissolution failure, pitting is inhibited and maintains a metastable state, or it is repaired. However, if the rate of pitting is higher than that of re-passivation, the alloy lose the protection of the passive film thoroughly. Therefore, the properties of the passive film strongly affect the pitting process. In addition, the passive film is determined by the alloy composition of the material when other factors are the same. The variation in Cr content of stainless steel brings composition segregation on the surface of the alloy and induces the defects of passive film. When the aggressive  $\text{Cl}^-$  ions preferentially attack the defects of passive film, as shown in Fig. 11 (a-1) and (b-1), the local electric field strength increases, which may eventually lead to a complete breakdown of the passive film and the formation of a pit[35], as shown in Fig. 11(a-2) and (b-2). The larger the variation in the level of Cr content is, the more inhomogeneity in the passive film; therefore, the protectiveness of the passive film becomes weak. Therefore, low  $E_p$  and  $R_{ct}$  values for the specimens with larger variations in the level of Cr content are obtained (Fig. 8 and 9). In addition, once the pits initiate, they can grow stably without re-passivation owing to the pitting rate being higher than the re-passivation rate, as shown in Fig. 11(b-3). Certainly, the Cr-depleted zones or boundaries of the sigma phase and secondary austenite are the most favourable sites for pit initiation because these locations have the most weakness in the passive film (seen in Fig. 10 (a-1), (b-1) and (c-2)). However, in specimens with small variations in the level of Cr content, re-passivation occurred due to the lower composition micro-segregation of Cr element, which makes a certain degree of protection of passive film relative, as shown in Fig. 11(a-3). Metastable pitting remains until higher potential is applied. Therefore, the charge transfers onto the surface of steels with small variation in the level of Cr content with difficulty, and higher  $R_{ct}$  and  $E_p$  are achieved, as shown in Fig. 8 and 9. Although more sigma phases produce more Cr-depleted zones, they do not all become the source of pitting, and the probability of pitting at preferential sites of Cr-depleted zone or boundaries of the sigma phase and secondary austenite in these specimens is smaller than that with larger variation in the level of Cr content, as shown in Fig. 10. Consequently, pitting corrosion of DSS induced by sigma precipitation directly contributed to the difference in Cr content between the sigma phase and Cr-depleted zone but not only to the Cr-depleted zone itself.

#### 4. CONCLUSIONS

1. Nearly identical variations in Cr content were obtained in three different DSS specimens, SAF2205, SAF2507 and Z3CN20.09M, which have nearly the same amount of sigma phases, using appropriate ageing and annealing technology.
2. The pitting potential of all three DSS specimens with small variations in the level of Cr

content is remarkably higher than that of specimens with larger variations in Cr content, although they contain almost the same sigma precipitates. Even if there is more sigma phase in specimens with smaller variations in Cr content, they still present more resistance to pitting corrosion by high  $E_p$  values.

3. With increasing variation in Cr content, the diameter of the depressed semicircle of Nyquist plots decreased. Lower  $R_{ct}$  values are observed in DSS specimens containing large variations in Cr content, representing an increased transport of ions through the double-charge layer, which indicates relatively poor resistance to corrosion.

4. In the specimens with larger variations in Cr content, more pits arose at and/or in the boundaries of austenite and ferrite in which the sigma phase precipitated. In other specimens with smaller variations in Cr content, however, fewer pits appeared at and/or in the boundaries of austenite and ferrite, although these specimens contain more sigma phases.

5. Pitting corrosion of DSS induced by sigma precipitation is mainly ascribed to the difference in Cr content between the sigma phase and Cr-depleted zone and not only to the Cr-depleted zone itself.

#### ACKNOWLEDGEMENTS

The authors are very grateful for the support from the National Natural Science Foundation of China under No. 51501001 and Anhui Provincial Natural Science Foundation under No. 1508085QE102.

#### References

1. G.S. Frankel, *J. Electrochem. Soc.*, 145 (1998) 2186.
2. P.C. Pistorius, G. T. Burstein, *Phil. Trans. R. Soc. Lond. A*, 341 (1992) 531.
3. M.P. Ryan, D.E. Williams, R.J. Chater, B.M. Hutton, D.S. McPhail, *Nature*, 415 (2002) 770.
4. G.S. Eklund, *J. Electrochem. Soc.*, 121 (1974) 467.
5. G. Wranglen, *Corros. Sci.*, 14 (1974) 331.
6. D.E. Williams, M.R. Kilburn, J. Cliff, G.I.N. Waterhouse, *Corros. Sci.*, 52 (2010) 3702.
7. D.E. Williams, Y.Y. Zhu, *J. Electrochem. Soc.*, 147 (2000) 1763.
8. J. Stewart, D.E. Williams, *Corros. Sci.*, 33 (1992) 457.
9. M.A. Baker, J.E. Castle, *Corros. Sci.*, 34 (1993) 667.
10. Z. Szklarska-Smialowska, Pitting corrosion of metals, *NACE*, (1986) *Houston, America*,.
11. Y.Q. Wang, N. Li, B. Yang, *Corros. Eng. Sci. Techn.*, 50 (2015) 330.
12. Y.Q. Wang, B. Yang, J. Han, H.C. Wu, X.T. Wang, *Mater. Trans.*, 54 (2013) 839.
13. Y.Q. Wang, D. D. Li, L. Sun, N. Li, M. K. Liu, W. Shen, H.M. Jing, *Corros. Eng. Sci. Techn.*, 52 (2017) 447.
14. N. Lopez, M. Cid, M. Puiggali, *Corros. Sci.*, 41 (1999) 1615.
15. K.N. Adhe, V. Kain, K. Madangopal, H.S. Gadiyar, *J. Mater. Eng. Perform.*, 5 (1996) 500.
16. H.M. Ezuber, A. El-Houd, F. El-Shawesh, *Desalination*, 207 (2007) 268.
17. L.H. Zhang, Y.M. Jiang, B. Deng, W. Zhang, J.L. Xu, J. Li, *Mater. Charact.*, 60 (2009) 1522.
18. J.O. Nilsson, *Mater. Sci. Techn.*, 8 (1992) 685.
19. K.H. Lo, C.H. Shek, J.K.L. Lai, *Mater. Sci. Eng. R.*, 65 (2009) 39.
20. Y.S. Ahn, J.M. Kim, B.H. Jeong, *Mater. Sci. Techn.*, 18 (2002) 383.
21. H. Tan, Y.M. Jiang, B. Deng, T. Sun, J.L. Xu, J. Li, *Mater. Charact.*, 60 (2009) 1049.
22. B. Deng, Z.Y. Wang, Y.M. Jiang, H. Wang, J. Gao, J. Li, *Electrochim. Acta.*, 54 (2009) 2790.

23. J.O. Nilsson, A. Wilson, *Mater. Sci. Tech.*, 9 (1993) 545.
24. R.N. Gunn, Duplex stainless steels: Microstructure, properties and applications, *Abington*, (1997) *Cambridge, England*.
25. R. Magnabosco, *Mater. Res.*, 12 (2009) 321.
26. Y.Q. Wang, J. Han, B. Yang, H.C. Wu, X.T. Wang, *Acta. Materialia Sin.*, 49 (2013) 415.
27. L.H. Zhang, W. Zhang, Y.M. Jiang, B. Deng, D.M. Sun, J. Li, *Electrochim. Acta.*, 54 (2009) 5387.
28. P. Bommersbach, C. Alemany-Dumont, J.P. Millet, B. Normand, *Electrochim. Acta.*, 51 (2005) 1076.
29. J.R. Macdonald, Impedance Spectroscopy—Emphasizing Solid Materials and Systems, *Wiley*, (1987) *New York, America*.
30. M. Kissi, M. Bouklah, B. Hammouti, M. Benkaddour, *Appl. Surf. Sci.*, 252 (2006) 4190.
31. W.S. Li, N. Cui, J.L. Luo, *Electrochim. Acta.*, 49 (2004) 1663.
32. C.O.A. Olsson, D. Landolt, *Electrochim. Acta.*, 48 (2003) 1093.
33. I. Olefjord, B. Elfstrom, *Corrosion.*, 38 (1982) 46.
34. J. Horvath, H. H. Uhlig, *J. Electrochem. Soc.*, 115 (1968) 791.
35. T.P. Hoar, D.C. Mears, G.P. Rothwell, *Corros. Sci.*, 5 (1965) 279.

© 2018 The Authors. Published by ESG ([www.electrochemsci.org](http://www.electrochemsci.org)). This article is an open access article distributed under the terms and conditions of the Creative Commons Attribution license (<http://creativecommons.org/licenses/by/4.0/>).